PAN
POLISH ACADEMY OF SCIENCES

Opto-Electronics Review

journal homepage: https://journals.pan.pl/opelre

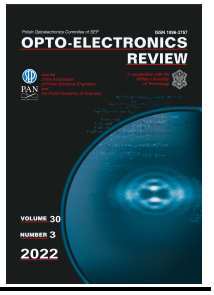

Imaging polarimeter with high-accuracy measuring principles in crystal optics

Mykola Shopa[a*], Serhiy Kobyakov[b], Yaroslav Shopa[b]

[a] Institute of Physics and Applied Computer Science, Gdańsk University of Technology, 11/12 Gabriela Narutowicza St., 80-233 Gdańsk, Poland
[b] Faculty of Mathematics and Natural Sciences, Cardinal Stefan Wyszyński University in Warsaw, 5 Dewajtis St., 01-815 Warsaw, Poland

Article info

Article history:
Received 18 Apr. 2022
Received in revised form 19 May 2022
Accepted 30 May 2022
Available on-line 29 Jun. 2022

Keywords:
Birefringence; crystal optics; high-accuracy universal polarimeter; imaging polarimeter; polarization.

Abstract

An imaging polarimeter based on the principles of high-accuracy polarimetry well known in crystal optics is proposed. The application of scientific digital cameras for performance light measurements leads to precise data on polarizers quality, i.e., maps of extinction ratio and transmission axis. Processing of numerous images, acquired at various settings in the polarizer-sample-analyser system, allows to determine the two-dimensional distribution of the phase retardation of birefringent plates. Several results of imaging polarimetry experiments on birefringent plates demonstrate the impact of multiple light reflections on the measured phase retardation values. Experimental data for $LiNbO_3$ and SiO_2 crystal plates have been presented, demonstrating the capabilities of the proposed type of imaging polarimeter in the crystal optics studies. This technique also allows the measurement of the eigen wave ellipticities, associated with the optical activity of crystals.

1. Introduction

There are many application problems, from space observations and remote sensing to microbiological research, where information on the spatial distributions of polarization is crucial [1]. Two-dimensional mapping of the state of light polarization plays an important role in the evaluation of the polarization optics elements, optoelectronic devices, studying mechanical stresses in transparent objects, etc.

The optical schemes and operation principles of imaging polarimeters can be different [2] but in most cases they are Stokes polarimeters which are designed to fully characterize the polarization state of light using four parameters, or Mueller polarimeters which are used for samples studying and representing their properties in the form of a 4×4 matrix [3–5]. The polarizing microscopes used to study objects with a very small retardation [6, 7] and to determine the absolute values of the optical retardation in crystals should also be mentioned [8].

*Corresponding author at: mykola.shopa@pg.edu.pl

To avoid mechanical moving elements, complex image processing methods using Fourier analysis [9] or polarizing cameras [10, 11] can be applied, although it is extremely difficult to obtain a high-quality micropolarizer on image sensor pixels [12, 13]. It is not the authors' purpose to present an in-depth overview, but note that the imaging polarimeter is an important optical tool for obtaining experimental data and its methods are constantly being improved.

This paper describes the application of an imaging polarimeter in a collection of two-dimensional spatial distributions of the polarization state using the principles of a high-accuracy universal polarimeter (HAUP) which have been successfully applied in the crystal optics research for several decades. It should be noted here that the imaging experiment, based on the HAUP, was initially proposed in Ref. 14 to produce maps of several anisotropic optical parameters by scanning procedure and was, therefore, called S-HAUP. A different approach to expand the possibilities of the high-accuracy polarimetry, using a charge-coupled device (CCD-HAUP), was proposed in Ref. 15.

https://doi.org/ 10.24425/opelre.2022.141948
1896-3757/ Association of Polish Electrical Engineers (SEP) and Polish Academic of Sciences (PAS). Published by PAS

The main idea of the high-accuracy polarimetry is to measure small changes in the polarization state of light that passes through the polarizer-sample-analyser (PSA) system, taking into account the systematic errors that arise mainly due to the imperfection of polarizers. In this case, polarizers angular movements do not exceed a few degrees from the position that corresponds to the minimum light intensity. This feature is important for accurate measurements since it is difficult to ensure the linearity of video detectors in a wide dynamic range of light flux changes.

Digital signal conversion of an analog video signal, even to a 12-bit depth, only makes sense if the signal-to-noise ratio is more than 72 dB which can only be provided by dedicated video cameras. It is known that photodiodes in the photovoltaic mode generate a current which is proportional to the light intensity over 6 decades [16], i.e., a dynamic range is about 120 dB. Therefore, a full implementation of the principles of high-accuracy polarimetry cannot be realized in imaging polarimeters, and this is due not only to the problem of accurate light detection.

Another not less significant hurdle to the application of high-accuracy polarimetry in a two-dimensional mode is the use of large-area polarizers with high transmission and extinction (or contrast) ratio (ER). For large-area dichroic polarizers with a clear aperture up to 50 mm, the ER value is relatively small, typically in the range from $1{:}10^2$ to $1{:}10^4$. At the same time, the magnitude of the systematic errors, related to imperfection of polarizers in a conventional HAUP, often makes it difficult to distinguish some important parameters of the optical anisotropy of crystals [17, 18].

Nevertheless, the imaging polarimeter can be successfully used to evaluate the quality of polarizers, and analyse the homogeneity of crystals and phase plates, light modulators, and others. This makes it possible to expand the capabilities of a conventional HAUP which is designed to solve similar problems on a single-beam track. Imaging polarimeters are significantly more informative, but they are inferior to HAUP in terms of sensitivity and measurement accuracy, so these two types of polarimeters complement each other.

2. Schematic of the imaging polarimeter

A schematic of the tested imaging polarimeter, based on the principles of the high-accuracy polarimetric method, is presented in Fig. 1. The optical design of the polarimeter is based on a standard PSA scheme. The quarter-wave plate is installed in front of the polarizer which makes the intensity of light at the output of the polarizer independent of its angular orientation. To obtain the spatial birefringence distribution with the proposed polarimetric method, a monochromatic light source is required.

The imaging polarimeter currently operates at a 633 nm helium-neon laser wavelength and is an upgrade of the previously used HAUP for research in crystal optics. The laser beam is expanded on a rotating ground glass diffuser followed by a lens with an outer diameter of 30 mm. The expanded parallel beam passes then through the polarizer, birefringent sample plate and analyser. Two motorized rotation mounts are used for the angular setting of the polarizer and analyser with a resolution of 0.01 deg or

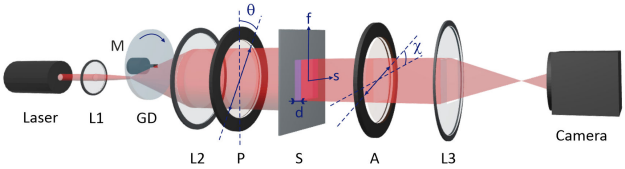

Fig. 1. Schematic representation of the imaging polarimeter and the light propagation through the polarizer P, sample S, and analyser A. L1, L2 are the laser beam expander; L3 – imaging lens; GD – ground glass diffuser; M – motor. Here, θ is the azimuth of the polarizer with respect to the crystal principal of fast f and slow s axes and χ is the azimuth of the analyser with respect to the crossed position with the polarizer, d is the sample thickness.

0.01/8 deg, using a micro-step adjustment for smoother rotation performed by the computer controlling system, while the sample stays static. The angle between the passing axis of the polarizer and analyser is initially close to 90 deg.

The expansion of the coherent laser light by a laser beam expander is usually accompanied by the appearance of a speckle pattern in the images. Therefore, a conventional way to eliminate coherent noise in the form of a rotating glass diffuser [19] mounted on a conventional 7200 rpm hard disk motor has been used.

After the light has passed through the PSA, the monochrome 5 MP CMOS camera BFLY-PGE-50S5M, equipped with a 58mm/0.5 lens detects the spatial distribution of the light intensity in the grayscale image keeping the sample in focus. Five dark frames are captured beforehand in complete darkness and average frames are subtracted further from each high dynamic range image in order to eliminate a constant digital camera noise. The transmitted light varies with position over the sample, but it does not affect the measured parameters of the polarimeter. However, any change in the laser intensity or drift in camera sensitivity during measurements results in measurement errors in the polarization state.

3. Experimental procedure

3.1. Map of the extinction ratio measurement

The light is partially polarized at the output of the imperfect polarizer. If such light then passes through an ideal polarizer (analyser), its rotation will cause intensity of the transmitted light to change in the range from $I_{\max}$ to $I_{\min}$ and a degree of the polarization P can be defined as [20]

$$P = \frac{I_{\max} - I_{\min}}{I_{\max} + I_{\min}}. \tag{1}$$

The polarization degree is related to the polarization extinction ratio

$$\eta = \frac{1 - P}{1 + P} \tag{2}$$

which is the ratio of the minimum transmission to the maximum transmission of the light when the analyser is rotated. This quantity is often used as a quality parameter of polarizing devices, and most often it should be as small

as possible. For commercial Glan-Thomson polarizers, the extinction ratio η is usually in the range from 10^{-6} to 10^{-5} and for a dichroic polarizing film from 10^{-4} to 10^{-2} [21]. It should be noted that the extinction ratio can also be expressed in decibels, particularly $\mathrm{ER} = 10\log\left(\frac{I_{\max}}{I_{\min}}\right)$, therefore, its value is always positive and is usually used to characterize light polarization in optical fibres [22].

To find both high and low extinction ratios, the maximum $I_{\max}$ and minimum $I_{\min}$ intensities should be measured which means that the analyser must perform a rotation within about 90 degrees. This measurement is difficult to carry out for small η values since it requires using light detectors with a high dynamic range. However, using the generalized Malus' law [23], it is possible to implement accurate measuring of the extinction ratio for small angles (± 2 deg) of the analyser rotation. When passing through the non-ideal polarizer, the light intensity, which corresponds to the transitions axis of the polarizers, remains unchanged, but the light intensity which corresponds to the perpendicular axis is attenuated by the factor η_1 in the polarizer and by η_2 in the analyser. Assuming that at the input to the polarizer-analyser (PA) system, the light intensity is equal to I_0, the output intensity I depends on the angle φ between the axes of the polarizer and the analyser as follows:

$$I(\varphi) = \frac{I_0}{2}[(1+\eta_1\eta_2)\cos^2\varphi + (\eta_1+\eta_2)\sin^2\varphi]. \quad (3)$$

Under the conditions of an ideal polarizer and analyser, this expression transforms into the well-known Malus' law. Usually, in the experimental setup both polarizers have similar extinction ratio values, then $\eta_1 = \eta_2 = \eta$ and, thus

$$I(\varphi) = \frac{I_0}{2}[(1+\eta^2)\cos^2\varphi + 2\eta\sin^2\varphi]. \quad (4)$$

Instead of the angle φ it is more convenient to use the misaligned angle $\alpha = \varphi - \pi/2$ between the crossed polarizer and analyser. It should be also taken into account that the position of the angle α, which corresponds to the minimum transmission of the PA system, is initially unknown and its nonzero value as α_0 is introduced. Then, assuming that $\alpha \ll 1$, the formula for intensity can be expressed in a parabolic form

$$I(\alpha) \approx \frac{I_0}{2}[(\alpha-\alpha_0)^2 + 2\eta] = a\alpha^2 + b\alpha + c, \quad (5)$$

where terms that are small by the order of magnitude and proportional to η^2 and α^4 are omitted, and a, b, c are the coefficients of the approximation parabola. It can be seen that the input intensity $I_0 = a$, the minimum intensity $I_{\min} = I(\alpha_0) = \eta I_0$, the angle α, which corresponds to the minimum intensity, is equal to $\alpha_0 = -b/2a$ and for the extinction ratio the following expression is obtained:

$$2\eta = \frac{c}{a} - \frac{b^2}{4a^2}. \quad (6)$$

In order to experimentally determine the extinction ratio η, the measurement range of α not larger than 0.05 rad is used. From (5) it follows that the light intensity after the analyser at the angle $\alpha - \alpha_0 = \sqrt{2\eta}$ is doubled compared to that at $\alpha - \alpha_0 = 0$. The error in the determination of η comes from the uncertainty in the measurement of the angle α and the light intensity. This fact imposes certain requirements on the resolution of the analyser rotation which must be sufficient to determine the expected 2η value for two identical polarizers.

A similar experimental technique was applied in Refs. 24 and 25 which show the possibility of the precise extinction ratio measurement in the region of the order of 10^{-10}.

In the following test, both the polarizer and the analyser were identical dichroic thin polarizing films with a diameter of 50 mm between two windows with a thickness of 3 mm each. To obtain a full map of the extinction ratio 2η, 25 images were achieved by changing the analyser position approximately from $\alpha = -2.0$ to $+2.0$ deg and with the polarizer standing still. As a pre-processing stage, the Gaussian filter with a standard deviation of 3 to 5 was used to blur each image which brings some loss of detail.

Figure 2 shows an example of measured data points for light intensity transmitted through the PA system as a

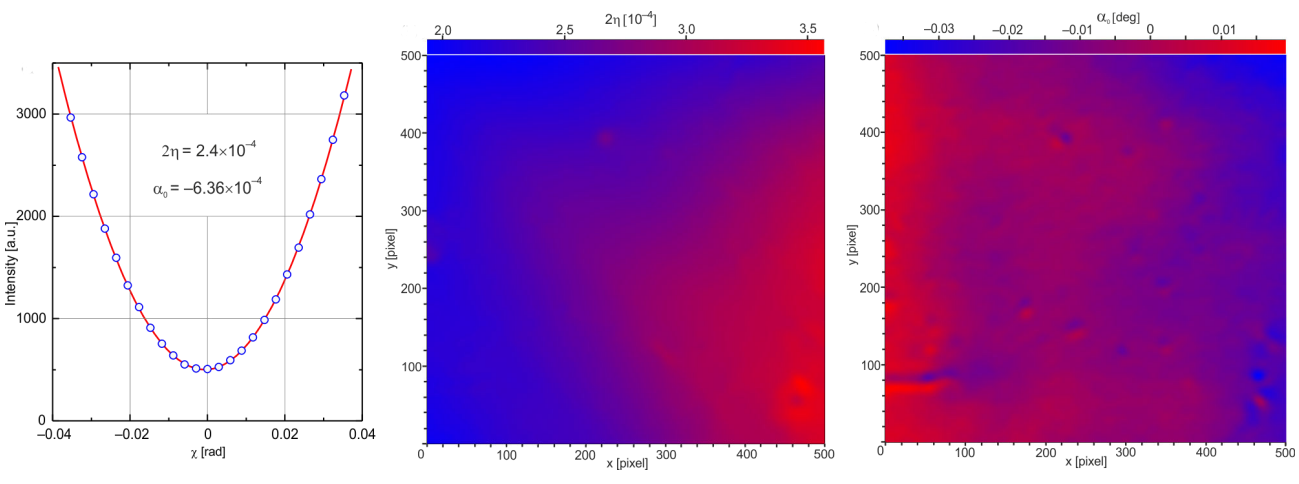

(a) (b) (c)

Fig. 2. The measurement results of parameters for two identical polaroids in PA system: dependence of the light intensity transmitted through PA system on the analyser azimuth χ for the pixel located at [386, 405] (a); spatial distribution of the extinction ratio $2\eta(x, y)$ (b); distribution of the angle $\alpha_0(x, y)$ that corresponds to the minimum intensity (c).

function of the analyser azimuth χ and a least-squares parabola based on the coefficients a, b, and, c according to (5). For the pixel located at [386, 405] in the image, the extinction ratio, found by curve fitting, equals $2\eta = (2.4 \pm 0.2) \times 10^{-4}$. A similar procedure for obtaining these coefficients of the approximation parabola was carried out for each pixel of a digital camera. This procedure made it possible to get a map of the extinction ratio, as well as the analyser azimuth α_0 which corresponds to the minimum light transmission in the PA system. The spatial distribution of the extinction ratio and the angle of the minimum intensity in Fig. 2 correspond to an area of approximately 15×15 mm^2. The extinction ratio, obtained this way for two polarizers, indicates the inhomogeneity of their polarization properties due to fabrication errors. Spatial distribution of the angle $\alpha_0(x, y)$ in Fig. 2(c) corresponds to the minimum intensity of the PA system (commonly termed crossed polarizers). In an ideal analyser, such distribution can be considered as a spatial distribution of polarization across the polarizer aperture or as a map of the main transmission axis of the tested linear polarizer.

3.2. *Phase difference measurement*

Let us now consider the analytic expression of the polarimeter. In high accuracy, polarimetry experiments are performed under the condition when the birefringent sample is placed between a nearly crossed polarizer and an analyser. At the same time, the azimuth θ of the polarizer with respect to the principal axis of the sample is small ($\theta \ll 1$). It is assumed that with crossed polarizers and $\theta = 0$, the analyser azimuth is also zero ($\chi = 0$). Under these conditions, the relative intensity of the transmitted light through the PSA system can be written in the simplified form of an elliptic paraboloid [26]:

$$J(\theta, \chi) = \theta^2 - 2\cos\Gamma \cdot \theta\chi + \chi^2 + 2k\sin\Gamma \cdot (\theta - \chi), \quad (7)$$

where $\Gamma = \frac{2\pi}{\lambda}\Delta n d$ is the phase difference between the two eigen waves of the light in the sample, λ is the wavelength of light, Δn is the linear birefringence (LB), and d is the sample thickness, k is the parameter that relates to the optical activity (OA) of the crystal which is defined as the ratio of the minor axis to the major axis of the ellipse of eigen waves polarization [27]. The actual azimuth θ differs from the measured azimuth θ' by the unknown value $\delta\theta$, so that $\theta = \theta' + \delta\theta$. Equation (7) does not take into account the imperfection parameters of polarizers which are important for the accurate determination of the k value, but do not affect the measured Γ value.

The phase difference Γ has been determined by a method similar to that used in a conventional polarimeter [26, 28]. The analyser azimuth $\chi_{\min}^{\mathrm{PSA}}$ that corresponds to the minimum of the light transmission through the PSA system can be obtained from the condition $(\partial J/\partial\chi)_\theta = 0$:

$$\chi_{\min}^{\mathrm{PSA}}(\theta', \Gamma) = (\theta' + \delta\theta)\cos\Gamma + k\sin\Gamma \quad (8)$$

In the PA system, the phase difference $\Gamma = 0$, and the experimental dependence $\chi_{\min}^{\mathrm{PA}}(\theta') = \theta'$ accordingly can be used as a reference line. Furthermore, it can be seen that in the PSA system, the intensity minima azimuths $\chi_{\min}^{\mathrm{PSA}}$ of the analyser are on a straight line with the slope equal to $\cos\Gamma$.

4. Imaging polarimetry for wave plates

Next, the rotating polarizers method was employed to get a 2D phase retardation distribution by the method used in the single-channel conventional polarimeter. To do this, the images obtained on the polarimeter at different relative positions of the polarizers are processed. Optimally, it was 81 or 121 HDR images, i.e., 9 or 11 positions for the polarizer and the analyser, respectively. The main procedure in further image processing is to find the minimum of the light intensity for each pixel of the sample image in the PSA system while rotating the analyser and keeping the polarizer still.

The most common type of wave plate is a quarter-wave plate, for which the phase difference is $\Gamma = \pi/2$ for a specific wavelength. Figure 3 plots the phase difference variation for a central part of the aperture of a commercial zero-order quarter-wave plate with a diameter of 50 mm fabricated for a 633 nm wavelength. The measured mean value of the phase difference throughout the wave plate is $\Gamma \approx \frac{\pi}{2} - 0.12$ and is relatively close to the ideal phase difference of $\Gamma_0 = \frac{\pi}{2}$. A difference of around $\Gamma - \Gamma_0 \approx -0.12$ rad is within tolerance for some applications of this type of wave plates. However, a more noticeable characteristic of the obtained distribution of the phase retardation is its spatial modulation with a depth of 10%, caused by the multiple reflections of light at the faces of the plate. The period of the spatial modulation is less than 2 mm and may remain unnoticed when using conventional polarimetric schemes with a narrow laser beam. In practice, it is difficult to position the light beam in such a way that the phase difference is constant when the experimental conditions are changing.

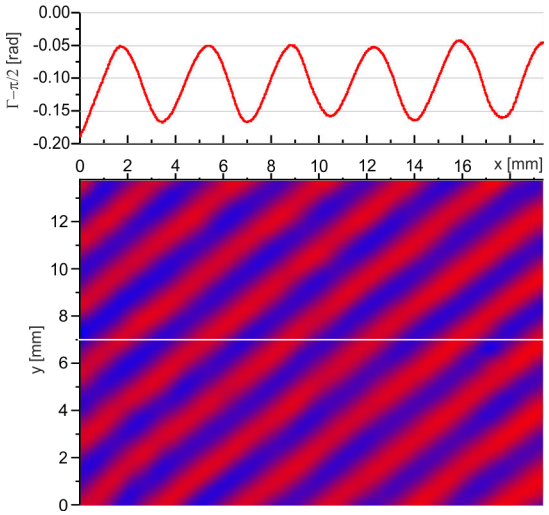

Fig. 3. Phase difference $\Gamma - \pi/2$ variation along the selected row of pixels (white line) for a quarter-wave plate made for a wavelength of 633 nm (top) and spatial distribution map of the phase difference (bottom).

A similar result was obtained for an quarter-wave plate but fabricated for a light wavelength of 450 nm (Fig. 4). The measured Γ value with a helium-neon laser varies from

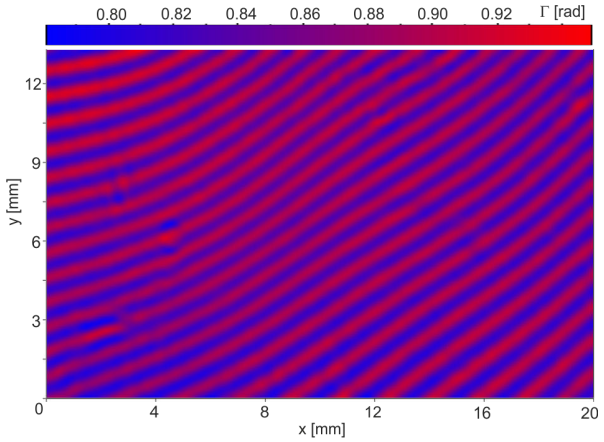

Fig.4. Spatial variation of the phase difference Γ map across the birefringent wave plate for a wavelength of 450 nm.

0.78 to 0.95 rad and is not close to $\pi/2$. These data were presented in order to exclude the influence of polarization elements on the observed pattern of spatial variations in the effective value of the phase difference. The modulation depth here is more significant and averages almost 20%. Obviously, the use of wave plates with such properties may be limited in systems with the spatial light modulation.

Retardance variations may be related to irregularities in crystal thickness and also influenced by multiple light reflections. Due to the relatively high refractive index of the lithium niobate crystal, the interference fringes of similar width are clearly visible. Figure 5 (top) shows in the insert one of the 121 converted to 8-bit grayscale images of the $LiNbO_3$ crystal plate with a size of 12×16 mm^2 and an average thickness of $d \approx 0.445$ mm. Based on (8), the measured value of the cosine of the phase difference Γ is equal to

$$\cos\Gamma_{\text{meas}} = \frac{\partial \chi_{\text{min}}^{\text{PSA}}}{\partial \theta'}, \tag{9}$$

and it does not take into account the influence of interference phenomena associated with the reflection of light in a crystal plate, thickness of which is not constant. Handmade crystalline plates usually have a maximum thickness in their centre and then it decreases towards the edge. Figure 5 (top) also shows the spatial variation of the measured $\cos\Gamma_{\text{meas}}$ value and transmitted light intensity along the row of pixels highlighted by the red dash line in the insert. The correlation between interference fringes and spatial variations of $\cos\Gamma_{\text{meas}}$ is clearly visible. A 3D surface plot of the $\cos\Gamma_{\text{meas}}$ for a central part of 6 × 5 mm^2 of the crystal plate was also shown in Fig. 5 (bottom). The procedures for correction of such results are described in detail in Ref. [29] where the effectiveness of the HAUP technique under similar experimental conditions is demonstrated by several examples. As follows from Refs. 29 and 30, in the polarimetric experiment, the maximum $\cos\Gamma_{\text{meas}}^{+}$ and minimum $\cos\Gamma_{\text{meas}}^{-}$ of the observed $\cos\Gamma_{\text{meas}}$ values correspond to extreme values of the interference factor $\cos 2\varphi = \pm 1$, where $\varphi = (2\pi/\lambda)\bar{n}d$, and $\bar{n}$ is the mean refractive index of the birefringent crystal plate. Then, the extremal values of the $\cos\Gamma_{\text{meas}}^{\pm}$ are related to the actual $\cos\Gamma$ value through the relation

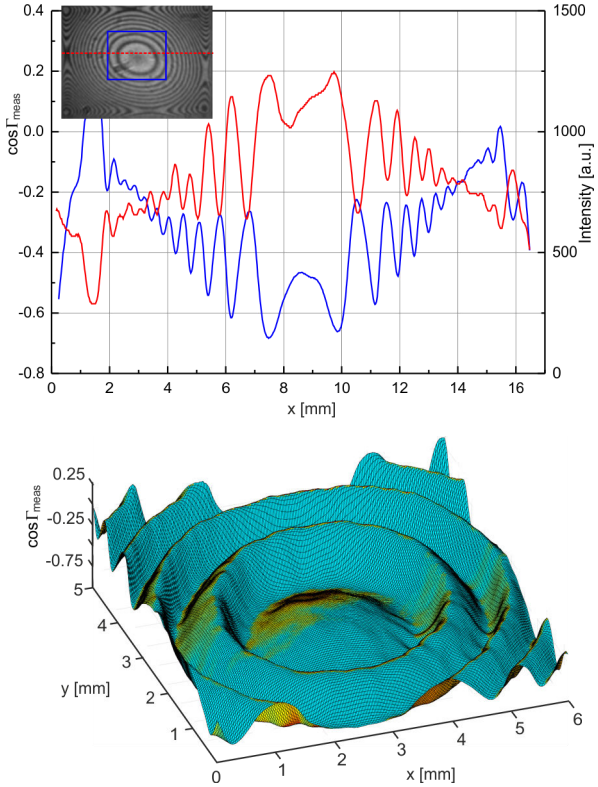

Fig.5. Spatial variation of the measured $\cos\Gamma_{\text{meas}}$ value (blue) and transmitted light intensity (red) along the row of pixels for crystal plate $LiNbO_3$ (a mean thickness of 445 μm). In the insert, there is one of 121 images of the $LiNbO_3$ crystal plate in the PSA system (top). 3D surface plot of the $\cos\Gamma_{\text{meas}}$ for a central part of the crystal plate selected with a blue rectangle area (bottom).

$$\cos\Gamma_{\text{meas}}^{\pm} = \frac{\cos\Gamma \pm 2r^2}{1 \pm 2r^2\cos\Gamma} \tag{10}$$

where $r^2 = (\bar{n}-1)^2/(\bar{n}+1)^2$. For the lithium niobate crystal $r^2 = 0.147$, therefore, instead of the actual value of $\cos\Gamma \approx -0.5$, (10) gives the maximum and minimum values of $\cos\Gamma_{\text{meas}} \approx -0.24$ and -0.69, respectively, which is in good agreement with those observed in the central part of Fig. 6. Applying similar calculations for a quartz quarter-wave plate ($r^2 = 0.046$), the actual difference of $\cos\Gamma_{\text{meas}}^{+} - \cos\Gamma_{\text{meas}}^{-} \approx 0.18$ can be observed in Fig. 3. It is clear that multiple light reflections in polarizers also affect measurement results and can often occur in polarimetric measurements, especially using polarizing cameras where this phenomenon cannot be controlled.

5. Estimation of the eigen waves ellipticity

The imaging polarimeter can be configured to determine the parameters of the optical anisotropy associated with the optical activity of crystals against the background of linear birefringence. The capabilities of the tested polarimeter to determine the crystal optical activity have been tested on the sample of a crystalline quartz plate which was cut at an angle of about 30 deg to the optical axis. The ellipticity k of normal waves [27] for this direction is almost one order of magnitude higher than for

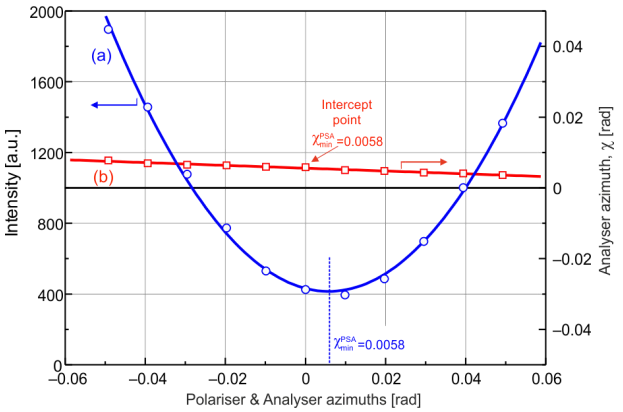

Fig. 6. An example of dependence of the light intensity transmitted for the one pixel through PSA system on the analyser azimuth χ^{PSA} (a). Dependence of $\chi^{\mathrm{PSA}}_{\mathrm{min}}$ on the polarizer azimuth θ', which was measured for a quartz plate with an average thickness of 1.75 mm (b).

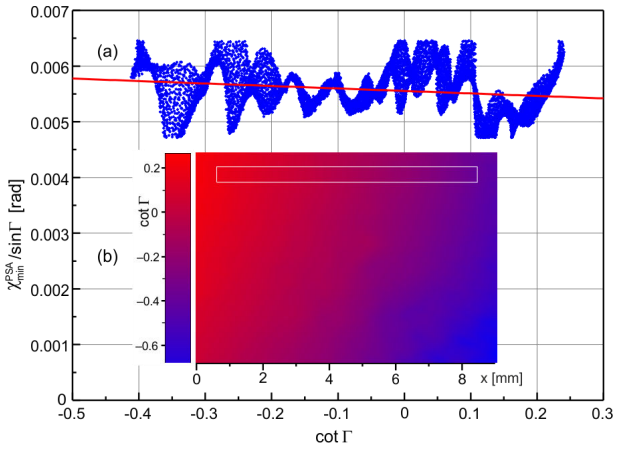

Fig. 7. The graph of intercept points from the linear dependence of $\frac{\chi^{\mathrm{PSA}}_{\mathrm{min}}}{\sin\Gamma}$ on $\cot\Gamma$ (in blue) and least squares best fit line (in red) (a). The $\cot\Gamma$ topology measured for a crystalline quartz plate (b). The area of $\cot\Gamma$ values that were used for least squares fitting is highlighted.

the direction perpendicular to the optical axis [31]. In this experiment, both the polarizer and the analyser were the Glan-Taylor calcite prisms with a 10 mm clear aperture and ER max. 1:10^5 [32]. This gives grounds to neglect the systematic errors of HAUP which in magnitude should be much smaller than the expected ellipticity, which in the described experiment was around $k \approx 0.006$.

If the sample is considered to be optically homogeneous (at least in terms of LB and OA), then the spatial changes in the maps of the phase difference Γ can be explained only due to the regular changes in the thickness d of the sample. For every pixel, the dependence of the light intensity, transmitted through the PSA system on the analyser azimuth χ^{PSA} can be obtained. Figure 6(a) shows an example of such dependence for one image pixel with the acquired analyser azimuth $\chi^{\mathrm{PSA}}_{\mathrm{min}}$. For the same pixel in Fig. 6(b), the experimental points of the analyser azimuth $\chi^{\mathrm{PSA}}_{\mathrm{min}}$ for each of the 11 positions of the polarizer are presented. According to (8), these points are on a straight line [red in Fig. 6(b)] with a slope equal to $\cos\Gamma$. Assuming in relation (8) the measured azimuth $\theta' = 0$, one can get

$$\frac{\chi^{\mathrm{PSA}}_{\mathrm{min}}(0,\Gamma)}{\sin\Gamma} = \delta\theta\cot\Gamma + k, \tag{11}$$

where $\chi^{\mathrm{PSA}}_{\mathrm{min}}(0,\Gamma)$ is the intercept point of the straight line $\chi^{\mathrm{PSA}}_{\mathrm{min}}(\theta',\Gamma)$ when $\theta' = 0$. Since the scan area and the step of the polarizer and analyser are the same, the horizontal axis in Fig. 6 is common. Dependence (10) can be experimentally found on the polarimeter for each image pixel using the above-mentioned spatial changes in the Γ quantity.

In can be seen in Fig. 7 that the slope of the best fit line $\frac{\chi^{\mathrm{PSA}}_{\mathrm{min}}}{\sin\Gamma}(0,\cot\Gamma)$ is the difference $\delta\theta = (4.45 \pm 0.20) \times 10^{-4}$ between the actual azimuth θ and the reading θ' on the polarimeter. The number of experimental points in this figure exceeds 10 000 and makes it possible to accurately estimate the magnitude of the eigenwaves ellipticity $k = (5.56 \pm 0.04) \times 10^{-3}$ in a quartz crystal which is related to optical activity. The oscillations in the graph are associated with the interference phenomenon in the crystal plate. When measured on a conventional polarimeter, the light beam passes through the sample at one point, therefore such dependencies are not observed. Naturally, for a direction that is perpendicular to the optical axis, this way of measurement of the k value should consistently take into account systematic errors of the polarization system. However, this does not exclude the fundamental possibility of using such a method for measuring OA.

6. Conclusions

Examples of using the principles of the conventional high-accuracy polarimetry well known in crystal optics have been presented in solving some problems in imaging polarimetry. To determine the main parameters of the elements of polarization optics, the basic relations known in HAUP are well suitable which makes it possible to use spatial variations of the phase difference due to insignificant changes in the thickness of the samples instead of changing their temperature. Small scanning angles of the polarizers azimuths can simplify the analytical expressions and also reduce the range of light intensity variation which improves the conditions of its measurement during the experiment. In this regard, this type of polarimeter is more advantageous when compared to the known schemes [1, 2] that use the extensive rotation (usually 0°, 45°, 90°, 135°) of polarizers.

Using the assumptions of the high-accuracy polarimetry in combination with modern imaging cameras, it is possible to obtain precise data on the quality of polarizers, in particular, maps of the extinction ratio and the main transmission axis.

The obtained experimental data for $LiNbO_3$ and SiO_2 crystal plates show sufficient sensitivity of the imaging polarimeter for the registration of multiple light reflections in birefringent plane-parallel plates, making it possible to quantify their spatial inhomogeneities. Such data can be used to test crystalline phase plates. The retardance and the orientation of the axis of birefringence can be measured by other methods, such as Refs. 33 and 35, but they require the introduction of additional phase elements which are sources of systematic errors in the high-accuracy

polarimetry. The ability to measure optical activity on the HAUP-type imaging polarimeter using the variation of the phase retardation in the sample is a significant advantage.

Authors' statement

Research concept and design, Y. S.; collection and assembly of data, M. S. and S. K.; data analysis and interpretation, Y. S., M. S., and S. K.; writing the article, M. S., S. K., and Y. S.; critical revision of the article, M. S.; final approval of article, M. S. and Y. S.

Acknowledgements

This research was funded in part by National Science Centre, Poland, grant No. 2021/41/B/ST3/00069. For the purpose of Open Access, the authors have applied a CC-BY public copyright license to any Author Accepted Manuscript (AAM) version arising from this submission.

References

[1] Tyo, J. S., Goldstein, D. L., Chenault, D. B. & Shaw, J. A. Review of passive imaging polarimetry for remote sensing applications. *Appl. Opt.* **45**, 5453–5469 (2006). https://doi.org/10.1364/AO.45.005453

[2] Chipman, R. A., Lam, W.-S. T. & Young, G. *Polarized Light and Optical Systems* (Boca Raton, CRC Press. 2018) https://doi.org/10.1201/9781351129121

[3] Azzam, R. M. A. Stokes-vector and Mueller-matrix polarimetry [Invited]. *J. Opt. Soc. Am. A.* **33**, 1396–1408 (2016). http://doi.org/10.1364/JOSAA.33.001396

[4] Goldstein, D. H. *Polarized light* (3rd ed.) Ch. 5–6 (Boca Raton, CRC press, 2017). https://doi.org/10.1201/b10436

[5] Pezzaniti, J. L. & Chipman, R. A. Mueller matrix imaging polarimetry. *Opt. Eng.* **34**, 1558–1568 (1995). https://doi.org/10.1117/12.206161

[6] Shribak, M. & Oldenburg, R. Techniques for fast and sensitive measurements of two-dimensional birefringence distributions. *Appl. Opt.* **42**, 3009–3017 (2003). https://doi.org/10.1364/AO.42.003009

[7] Shribak, M. Polychromatic polarization microscope: bringing colors to a colorless world. *Sci. Rep.* **5**, 17340 (2015). https://doi.org/10.1038/srep17340

[8] Geday, M. A., Kaminsky, W., Lewis, J. G. & Glazer, A. M. Images of absolute retardance L·Δn, using the rotating polariser method. *J. Microsc.* **198**, 1–9 (2000). https://doi.org/10.1046/j.1365-2818.2000.00687.x

[9] Oka, K. & Kaneko, T. Compact complete imaging polarimeter using birefringent wedge prisms. *Opt. Express* **11**, 1510–1519 (2003). https://doi.org/10.1364/OE.11.001510

[10] Rubin, N. A. *et al*. Matrix Fourier optics enables a compact full-Stokes polarization camera. *Science* **365**, 43–52 (2019). https://doi.org/10.1126/science.aax1839

[11] Gottlieb, D. & Arteaga, O. Mueller matrix imaging with a polarization camera: application to microscopy. *Opt. Express.* **29**, 34723–34734 (2021). https://doi.org/10.1364/OE.439529

[12] Sasagawa, K. *et al*. Image sensor pixel with on-chip high extinction ratio polarizer based on 65-nm standard CMOS technology. *Opt. Express.* **21**, 11132–11140 (2013). https://doi.org/10.1364/OE.21.011132

[13] Hagen, N. A., Shibata, S. & Otani, Y. Calibration and performance assessment of microgrid polarization cameras. *Opt. Eng.* **58**, 082408 (2019). https://doi.org/10.1117/1.OE.58.8.082408

[14] Kaminsky, W., Claborn, K. & Kahr, B. Polarimetric imaging of crystals. *Chem. Soc. Rev.* **33**, 514–525 (2004). http://doi.org/10.1039/b201314m

[15] Takanabe, A., Koshima, H. & Asahi, T. Fast-type high-accuracy universal polarimeter using charge-coupled device spectrometer. *AIP Adv.* **7**, 025209 (2017). https://doi.org/10.1063/1.4977440

[16] *Op Amp Applications Handbook* (ed. Yung, W. G.) (Analog Devices, 2002). http://www.miedema.dyndns.org/co/2018/Op_Amp_Applications_Handbook-Walt-Jung_2005.pdf

[17] Kobayashi, J. & Uesu, Y. A new optical method and apparatus HAUP for measuring simultaneously optical activity and birefringence of crystals. I. Principles and construction. *J. Appl. Crystallogr.* **16**, 204–211 (1983). https://doi.org/10.1107/S0021889883010262

[18] Hernández-Rodríguez, C., Gomez-Garrido, P. & Veintemillas, S. Systematic errors in the high-accuracy universal polarimeter: application to the determining temperature-dependent optical anisotropy of KDC and KDP crystals. *J. Appl. Crystallogr.* **33**, 938–946 (2000). http://doi.org/10.1107/S0021889800003605

[19] Stangner, T., Zhang, H., Dahlberg, T., Wiklund, K. & Andersson, M. Step-by-step guide to reduce spatial coherence of laser light using a rotating ground glass diffuser. *Appl. Opt.* **56**, 5427–5435 (2017). https://doi.org/10.1364/AO.56.005427

[20] Bennett, J. M. Polarization. in *Handbook of Optics* (eds. Bass, M., Van Stryland, E .W., Wolfe, W. L. & Williams, D.R.) vol. 1, Ch 5 (McGraw-Hill, 1995).

[21] Bennett, J. M. Polarizers. in *Handbook of Optics* (eds. Bass, M., Van Stryland, E. W., Wolfe, W. L. & Williams, D. R.) vol. 2, Ch. 3 (McGraw-Hill, 1995).

[22] Zhou, K., Simpson, G., Chen, X., Zhang, L. & Bennion, I. High extinction ratio in-fiber polarizers based on 45° tilted fiber Bragg gratings. *Opt. Lett.* **30**, 1285–1287 (2005). https://doi.org/10.1364/OL.30.001285

[23] Ratajczyk, F. Generalized Malus law. *Opt. Appl.* **9**, 281–283 (1979). https://opticaapplicata.pwr.edu.pl/files/pdf/1979/no4/optappl_904p281.pdf

[24] Takubo, Y., Takeda, N., Huang, J. H., Muroo, K. & Yamamoto, M. Precise measurement of the extinction ratio of a polarization analyser *Meas. Sci. Technol.* **9**, 20–23 (1998). https://doi.org/10.1088/0957-0233/9/1/004

[25] Mei, H.-H., Chen, Sh.-J. & Ni, W.-T. Suspension of the fiber mode-cleaner launcher and measurement of the high extinction-ratio (10^{-9}) ellipsometer for the Q & A experiment. *J. Phys. Conf. Ser.* **32**, 236–243 (2006). https://doi.org/10.1088/1742-6596/32/1/035

[26] Shopa, Y., Shopa, M. & Ftomyn, N. Dual-wavelength laser polarimeter and its performance capabilities. *Opto-Electron. Rev.* **25**, 6–9 (2017). http://doi.org/10.1016/j.opelre.2017.01.001

[27] Yariv, A. & Yeh, P. *Optical Waves in Crystals: Propagation and Control of Laser Radiation*. (Wiley, 2002).

[28] Shopa, M., Ftomyn, N. & Shopa, Y. Dual-wavelength polarimeter application in investigations of the optical activity of a langasite crystal. *J. Opt. Soc. Am. A* **34**, 943–948 (2017). https://doi.org/10.1364/JOSAA.34.000943

[29] Shopa, M. & Ftomyn, N. Application of two-dimensional intensity maps in high-accuracy polarimetry. *J. Opt. Soc. Am. A* **36**, 485–491 (2019). https://doi.org/10.1364/josaa.36.000485

[30] Hernández-Rodríguez, C. & Gomez-Garrido, P. Optical anisotropy of quartz in the presence of temperature-dependent multiple reflections using a high-accuracy universal polarimeter. *J. Phys. D* **33**, 2985–2994 (2000). https://doi.org/10.1088/0022-3727/33/22/318

[31] Konstantinova, A. F., Evdishchenko, E. A. & Imangazieva, K. B. Manifestation of optical activity in crystals of different symmetry classes. *Crystallogr. Rep.* **51**, 998–1008 (2006). https://doi.org/10.1134/S1063774506060113

[32] Crystal polarizers, *Thorlabs, Inc.* https://www.thorlabs.com/navigation.cfm?guide_id=2458 (2022).

[33] Shribak, M., Otani, Y. & Yoshizawa, T. Return-path polarimeter for two-dimensional birefringence distribution measurement. *Proc. SPIE*. **3754**, 144–149 (1999). https://doi.org/10.1117/12.366325

[34] Noguchi, M., Ishikawa, T., Ohno, M. & Tachihara, S. Measurement of 2D birefringence distribution. *Proc. SPIE*. **1720**, 367–378 (1992). https://doi.org/10.1117/12.132143

[35] Otani, Y., Shimada, T., Yoshizawa, T. & Umeda, N. Two-dimensional birefringence measurement using the phase shifting technique. *Opt. Eng.* **33**, 1604–1609 (1994). https://doi.org/10.1117/12.168435